Exchange-Dominated Pure Spin Current Transport in Alq_{3} Molecules

S. W. Jiang, S. Liu, P. Wang, Z. Z. Luan, X. D. Tao, H. F. Ding, and D. Wu

Phys. Rev. Lett. **115**, 086601 — Published 21 August 2015
DOI: 10.1103/PhysRevLett.115.086601

Exchange-dominated pure spin current transport in Alq_3 molecules

S. W. Jiang,[1] S. Liu,[1] P. Wang,[1] Z. Z. Luan,[1] X. D. Tao,[1] H. F. Ding,[1,2,*], D. Wu[1,2,*]

[1]*National Laboratory of Solid State Microstructures and Department of Physics, Nanjing University, 22 Hankou Road, Nanjing 210093, P. R. China*

[2]*Collaborative Innovation Center of Advanced Microstructures, Nanjing University, 22 Hankou Road, Nanjing 210093, P. R. China*

*Corresponding author: dwu@nju.edu.cn, hfding@nju.edu.cn

We address the controversy over the spin transport mechanism in Alq_3 utilizing spin pumping in the $Y_3Fe_5O_{12}$/Alq_3/Pd system. An unusual angular dependence of the inverse spin Hall effect is found. It, however, disappears when the microwave magnetic field is fully in the sample plane, excluding the presence of the Hanle effect. Together with the quantitative temperature-dependent measurements, these results provide compelling evidence that the pure spin current transport in Alq_3 is dominated by the exchange-mediated mechanism.

PACS numbers: 72.25.Dc, 72.25.Pn, 85.65.+h

The study of spin injection, transport and detection in organic semiconductors (OSCs) has drawn great interest owning to their strong potentials in spintronics application as well as the fundamental understanding of the spin transport mechanism.[1] The injection and detection of spin-polarized carriers in OSCs were successfully demonstrated by various approaches such as two-photon photoemission,[2] muon spin rotation,[3] spin-polarized organic light emitting diodes,[4] and isotope effect.[5] Despite rapid experimental progress, the basic mechanism remains debated.[6,7] For instance, even though the observation of giant magnetoresistance (MR) in organic spin valves (OSV) requires spin injection, transport, and detection by electrical means,[8] it has still been argued that the MR may originate from spin transport through pinholes, tunneling MR, or tunneling anisotropic MR rather than giant MR.[9,10] The presence of the Hanle effect is considered to be the proof of electrical spin detection.[11] (The Hanle effect has been used to prove electrical spin detection in inorganic materials.[12,13,14]) Despite many attempts, no clear evidence is shown for the presence of the Hanle effect in OSV.[15,16] To explain this, a new theory was proposed[17] that differs from prior hopping-based proposals, such as the hyperfine interaction (HFI)[18,19] and the spin-orbit coupling (SOC).[20] It suggests that the spin transport is due to an exchange-interaction between polarons, which is much faster than the carrier mobility. Therefore, a much stronger magnetic field is needed to observe the Hanle effect than that estimated from the carrier mobility. Experimental evidence of the exchange-mediated mechanism, however, is still missing.

A relatively new development in spintronics is the generation, propagation and detection of the pure spin current.[21] A pure spin current is a flow of spin angular momentum without an accompanying charge current. It opens new opportunities to create spin-based devices of low energy consumption.[22,23] Moreover, the pure spin current can be efficiently injected into semiconductors to circumvent the conductivity mismatch problem.[24] Recently, a pure spin current generated by ferromagnetic resonance (FMR) excitation of a permalloy electrode, known as the spin pumping effect, was demonstrated to be injected into and propagate in a semiconducting polymer and then detected by Pt via the inverse spin Hall effect (ISHE).[25] In the measurements, the authors found an interesting angular dependence of the ISHE voltage V_{ISHE} and explained it with the Hanle effect.[17]

In this Letter, we demonstrate an exchange-dominated pure spin current transport in the small molecule tris-(8-hydroxyquinoline) aluminum (Alq_3) pumped from $Y_3Fe_5O_{12}$ (YIG) and detected by Pd via the ISHE. For a large sample placed on top of a coplanar waveguide (CPW), we observed an unusual angle dependence of V_{ISHE}. For a control sample with size smaller than the signal-line width, this unusual angle dependence disappeared. Only a cosine angular dependence is found when the magnetic field ***H*** rotates out of the sample plane. When ***H*** rotates within the sample plane, it follows a cosine cubic function. The findings exclude the Hanle effect as the origin of the unusual angle dependence of V_{ISHE} in large samples. Furthermore, we find that V_{ISHE} is almost independent on temperature T=8-300 K, which is only expected for exchange-mediated spin transport. Our findings evidence that the pure spin current transport in Alq_3 is dominated by the exchange-mediated mechanism.

We chose YIG as the pure spin current source due to its extremely low damping.[26,27] A 4-μm-thick single-crystalline YIG film was grown on a $Gd_3Ga_5O_{12}$ (GGG) (111) substrate by liquid phase epitaxy with a roughness of ~0.6 nm.[28] We re-used the same YIG film multiple times without any apparent degradation in the measurements after ultrasonically cleaning it in acetone, ethanol and deionized water in sequence. The Alq_3 films were thermally evaporated at room temperature at a rate of 0.06 nm/s. Without breaking vacuum, a 10-nm-thick Pd stripe (0.1×4 mm^2) was deposited through a shadow mask by indirect *e*-beam evaporation as it can significantly reduce the penetration of metal atoms into an OSC and improve the sample reproducibility.[43] To rule out the possibility of the formation of pinholes in Alq_3, a $La_{0.7}Sr_{0.3}MnO_3$/Alq_3 (20 nm)/Pd control sample with the same active area was fabricated. Similar as the previous reports,[15] the current-voltage curves exhibit linear behavior at low voltage (<0.1 V), and non-linear behavior at high voltage (>0.1 V),[28] indicating the pinhole-free Alq_3 layer. From the linear region, we estimate the polaron concentration to be 10^{18}-10^{19} cm^{-3}, comparable to the estimation from the electron spin resonance (ESR) measurements.[28]

Figure 1 shows a schematic illustration of the spin pumping induced spin injection, transport and detection in a YIG/Alq_3/Pd device. The YIG magnetic moment $\boldsymbol{M}$ precesses upon microwave excitation. The precession pumps a pure spin current $\boldsymbol{j}_s$ into the adjacent Alq_3 layer.[24,25] The pure spin current has its spin axis $\boldsymbol{\sigma}$ parallel to precession axis. After propagation and relaxation in Alq_3, $\boldsymbol{j}_s$ is converted into a charge current $\boldsymbol{j}_c$ via the ISHE in Pd. The lock-in amplifier picks up a voltage signal $V_{ISHE} \propto \boldsymbol{j}_c$. The samples were placed upside down in the center of a CPW and electrically isolated from CPW by a polymer solder resist layer. As depicted in Fig. 1, θ_H and φ_H are defined as the angles between $\boldsymbol{H}$ and the x-axis in the xz-plane and xy-plan, respectively. The CPW comprises a 1-mm-wide signal line with 0.12-mm-wide gaps between the signal- and ground-lines. The microwave signal was modulated at 51.73 kHz.

Figure 2(a) presents the microwave absorption spectra extracted from the transmission coefficient (ΔS_{21}) of the scattering parameters for YIG/Alq_3 (50 nm)/Pd at frequency $f = 5$ GHz and input power $P_{in} = 1$ mW, with $\boldsymbol{H}$ applied along x-axis at room temperature. Figure 2(b) shows V_{ISHE} for the same sample at $f = 5$ GHz and $P_{in} = 540$ mW at room temperature. A voltage signal is observed around the resonance field $H_r \approx 1.10$ kOe, while no signal was observed in a YIG/Alq_3 (50 nm)/Cu (10 nm) control sample [Fig. 2(c)], indicating that V_{ISHE} is induced by the spin pumping from YIG and ISHE of Pd. V_{ISHE} is proportional to P_{in} for $f = 5$ GHz [Insert of Fig. 2(b)]. This is consistent with a direct-current spin-pumping model and indicates that the system is in the linear regime.[44,45]

In spin pumping measurements, several artificial signals could be induced by either the magnetoelectric or thermoelectric effects.[45-48] We excluded these artifacts as follows. First, since the Alq_3 layer between YIG and Pd is relatively thick, a proximity-induced ferromagnetic Pd is unlikely; hence, magnetoelectric effects, such as the spin rectification effect, anomalous Hall effect, or anomalous Nernst effect in Pd can be ruled out. Secondly, the Seebeck effect depends on the temperature gradient ∇T but not ***H***. V_{ISHE} is observed to reverse sign when ***H*** changes its direction 180° [Fig. 2(b)], ruling out the Seebeck effect. In fact, such behavior is a characteristic of the spin-pumping-induced ISHE.[49] Thirdly, a 20-nm-thick MgO layer is inserted between YIG and Alq_3, which is thick enough to block the spin current while the in-plane ∇T induced by the spin-wave heat conveyor[50] on YIG is maintained in Pd. The voltage signal disappears with the MgO insertion [Fig. 2(c)], ruling out the spin-wave heat conveyor effect induced Seebeck effect. In addition, the *f*-dependent measurement can be fitted to the Kittel formula:[51] $f = (\gamma / 2\pi)\sqrt{H_{\mathrm{r}}(H_{\mathrm{r}} + 4\pi M_{\mathrm{s}})}$, where γ is the gyromagnetic ratio and M_{s} is the saturation magnetization.[28] γ=1.72×10^{11} $T^{-1}s^{-1}$ and $4\pi M_{\mathrm{s}} = 0.196\,\mathrm{T}$ were obtained from the fitting, which are consistent with the material parameters of YIG,[52] indicating that V_{ISHE} is related to the YIG FMR. ∇T on YIG can be generated by the microwave heating in resonance condition, resulting in the spin Seebeck effect (SSE) in YIG[53] and hence additional ISHE voltage. Since ∇T is sensitive to the environment, the SSE is expected to have strong *T* dependence.[28] As will be discussed below, our measured signal is almost independent on *T*, suggesting the negligible contribution from the SSE. Therefore, we can identify the observed signal as being mainly caused by the spin-pumping-induced ISHE.

Figures 3(a) and (b) show the angular dependent V_{ISHE} with ***H*** rotating within the *xz*-plane (θ_H-scan) and *xy*-plan (φ_H-scan), respectively. In the θ_H-scan, we find the differences from previous reports for inorganic systems.[45] When ***H*** is tilted out-of-plane, ***M*** is no longer collinear with ***H*** due to the shape anisotropy, *i.e.*, $\theta_M \neq \theta_H$, in which θ_M is the angle between ***M*** and sample plane.[28] We take this into account and find that $V_{\rm ISHE}$ still cannot be described by a $\cos\theta_M$ function expected for ISHE.[45] We note that a similar unusual angular dependence of $V_{\rm ISHE}$ was also observed in the previous report, which attributed it to the Hanle effect.[25] The findings were highlighted as "the first and clear fingerprint of the precessional nature of polaron spins in an applied magnetic field".[54] The Hanle effect would suggest that the spin transport is not caused by the exchange mechanism.[17] The authors, however, found a sizeable signal and attributed its origin to the exchange mechanism.[25]

To crosscheck, we performed similar measurements with $\boldsymbol{H}$ rotating within the *xy*-plane. In such a geometry, $\boldsymbol{M}$ should be parallel to $\boldsymbol{H}_{\rm r}(>1\,{\rm kOe})$, *i.e.*, $\varphi_M \cong \varphi_H$, because the crystalline anisotropy of YIG is weak. This means that the Hanle effect should disappear. Our measurements, however, show that $V_{\rm ISHE}$ still cannot be fitted by a $\cos\varphi_M$ function well [Fig. 3(b)]. This strongly suggests that the unusual angular dependence of $V_{\rm ISHE}$ does not originate from the Hanle effect.

Organic materials typically cannot sustain the photolithography process, meaning relatively large sample size. As shown in Fig. 3(c), the active area of our YIG/Alq_3/Pd device is ~4×0.1 mm^2, which is much larger than the CPW signal-line width. The microwave magnetic field $\boldsymbol{h}$ should be non-uniformed in the sample. To check this, we performed a numerical simulation, using HFSS (High Frequency Structure Simulator, Ansoft Corp.), shown in Fig. 3(d). Indeed, we find that the magnitude and direction of $\boldsymbol{h}$ varies dramatically around the gap between the signal- and ground-lines. By assuming the YIG film is placed in the center of the CPW and ~0.1 mm above it, we estimate the ratio of the effective power with $\boldsymbol{h}$ acting on the *y*-direction and *z*-direction $P_y : P_z$ to be: 1:2.8, where $P_{y(z)} \propto \int_{V_{\rm YIG}} \boldsymbol{h}_{y(z)}^2 dV$.

In FMR, the procession of $\boldsymbol{M}$ can only be excited by the component of $\boldsymbol{h}$ perpendicular to it, $\boldsymbol{h}_\perp = \boldsymbol{h} \times \boldsymbol{M}/M$, with the corresponding microwave power $P_\perp \propto \int_{V_{\rm YIG}} \boldsymbol{h}_\perp^2 dV$. Since $\boldsymbol{j}_{\rm s}$ is along the *z*-direction and $\boldsymbol{\sigma}$ is parallel to $\boldsymbol{M}$ of YIG,

V_{ISHE} for $\boldsymbol{H}$ rotating in *xz*-plane and *xy*-plane can be expressed as:

$$V_{ISHE} \propto P_{\perp} |\boldsymbol{J_s} \times \boldsymbol{\sigma}|_y \propto P_y \cos\theta_M + P_z \cos^3\theta_M \, , \qquad (1)$$

and

$$V_{ISHE} \propto P_{\perp} |\boldsymbol{J_s} \times \boldsymbol{\sigma}|_y \propto P_y \cos^3\varphi_M + P_z \cos\varphi_M \, , \qquad (2),$$

respectively. Utilizing Eq. (1) and (2), we fitted our measured data [Fig. 3(a) and (b)]. The fittings reproduce the measured data well. They yield $P_y : P_z$ to be 1:2.9 and 1:2.3 for the θ_H-scan and φ_H-scan, respectively. Both agree with the estimated value of 1:2.8, suggesting that the angular dependence of V_{ISHE} originates from the non-uniform microwave field rather than from the Hanle effect.

From Eq. (1) and (2), we learn that the angular dependence of V_{ISHE} would be significantly different if the microwave is only excited in one direction. For instance, if only P_y exists, V_{ISHE} will have a $\cos\theta_M$ dependence in a θ_H-scan but a $\cos^3\varphi_M$ dependence in a φ_H-scan. To demonstrate this, the same device structure with an active area smaller than the signal line was fabricated. To achieve this, two 30-nm-thick MgO pads separated by a 0.3-mm-wide gap were deposited by *e*-beam evaporation using a shadow mask before depositing Alq_3 and Pd. This makes the sample's active area to be ~0.3×0.1 mm^2, which is smaller than the CPW signal line, as depicted in Fig. 4(c). In this case, $\boldsymbol{h}$ should be almost uniform in the sample along the *y*-direction. Figures 4(a) and (b) show the measured angular dependence of V_{ISHE} similar as in Figs. 3(a) and (b) but with smaller sample size. Indeed, the angle dependence can be fitted by $\cos\theta_M$ in the θ_H-scan and $\cos^3\varphi_M$ in the φ_H-scan, as shown in Figs. 4(a) and (b). These results confirm that there is no Hanle effect in the pure spin transport in Alq_3. The absence of the Hanle effect suggests the pure spin transport is not dominated by the hoping transport based mechanisms, since the Hanle effect would be expected. Instead, it is consistent with the recently proposed exchange-mediated mechanism.[17]

To further understand the underlying mechanism, we performed T-dependent measurements. The spin diffusion length λ_s for the HFI mechanism is expected to increase with increasing T,[19,20] while λ_s for the SOC mechanism is predicted to decreases with increasing T when T<80 K for Alq_3.[20,55] The exchange-mediated spin diffusion mechanism relies on quantum mechanical exchange coupling of spins that come close to each other on adjacent sites. It does not require physical carrier hopping, meaning that λ_s is much less T-dependent. Therefore, we studied the Alq_3 thickness (t) and T dependence of the normalized signal $\tilde{V}_{\mathrm{ISHE}}$, defined as V_{ISHE} normalized by the microwave absorption. $\tilde{V}_{\mathrm{ISHE}}$ decreases significantly with increasing t at T=300 K, shown in Fig. 5(a). The spin current is expected to decay exponentially with t,[8] $j_s = j_s(0)e^{-t/\lambda_s}$. From the fitting, we obtained λ_s ~50 nm at T=300 K, which is comparable with the value measured in Alq_3-based OSV at low temperature.[8]

In Fig. 5(b), we show the typical T-dependent $\tilde{V}_{\mathrm{ISHE}}$ for samples with various Alq_3 thickness (f=5 GHz, P_{in}=540 mW and θ_H=0°). The results were normalized to $\tilde{V}_{\mathrm{ISHE}}$ at 8 K. It remains almost unchanged with increasing T. We further extract λ_s at different T and it is almost independent on T [Inset of Fig. 5(b)]. This finding excludes the SOC and the HFI as the dominant mechanism for the spin relaxation in Alq_3 since both involve T-dependent carrier hopping.[18,20] Our results are consistent with the exchange-mediated mechanism in which spin transport is via the exchange between the localized carriers rather than hopping.[17] The estimated polaron concentration, 10^{18}-10^{19} cm^{-3}, also fulfills the condition required for the exchange mechanism.[17] In this model the spin is conserved and does not relax during the transport process, similar to spin-wave spin current transport in a magnetic insulator.[23] Therefore, λ_s is only determined by the spin relaxation time of the local carriers, which is T-independent, as measured by ESR and spin-$\frac{1}{2}$ photoluminescence-detected magnetic resonance.[56,57] Moreover, this mechanism suggests that the Hanle effect cannot be observed,[17] consistent with our experimental finding.

In summary, we demonstrate the injection of a pure spin current into Alq_3 from the ferromagnetic insulator YIG utilizing the spin pumping approach from 8 to 300 K. λ_s in Alq_3 is determined to be ~50 nm in this temperature range. V_{ISHE} shows an unusual angle dependence for large samples only. By comparing the results obtained with small samples, we identified the unusual angular dependence as originating from the non-uniformity of the microwave magnetic field of the CPW rather than the Hanle effect. The absence of the Hanle effect and temperature independence of λ_s strongly support that the pure spin current transport in Alq_3 is dominated by exchange coupling between carriers.

This work was supported by the National Basic Research Program of China (2013CB922103 and 2010CB923401), the NSF of China (11222435, 51471086 and 11374145) and the NSF of Jiangsu Province (BK20130054).

References:

[1] V. A. Dediu, L. E. Hueso, I. Bergenti, and C. Taliani, Nat. Mater. **8**, 707 (2009).

[2] M. Cinchetti, K. Heimer, J.-P. Wüstenberg, O. Andreyev, M. Bauer, S. Lach, C. Ziegler, Y. Gao, and M. Aeschlimann, Nat. Mater. **8**, 115 (2009).

[3] A. J. Drew, J. Hoppler, L. Schulz, F. L. Pratt, P. Desai, P. Shakya, T. Kreouzis, W. P. Gillin, A. Suter, N. A. Morley, V. K. Malik, A. Dubroka, K. W. Kim, H. Bouyanfif, F. Bourqui, C. Bernhard, R. Scheuermann, G. J. Nieuwenhuys, T. Prokscha, and E. Morenzoni, Nat. Mater. **8**, 109 (2009).

[4] T. D. Nguyen, E. Ehrenfreund, and Z. V. Vardeny, Science **337**, 204 (2012).

[5] T. D. Nguyen, G. Hukic-Markosian, F. Wang, L. Wojcik, X.-G. Li, E. Ehrenfreund, and Z. V. Vardeny, Nat. Mater. **9**, 345 (2010).

[6] C. Boehme and J. M. Lupton, Nat. Nanotechnol. **8**, 612 (2013).

[7] V. A. Dediu and A. Riminucci, Nat. Nanotechnol. **8**, 885 (2013).

[8] Z. H. Xiong, D. Wu, Z. V. Vardeny, and J. Shi, Nature **427**, 821 (2004).

[9] T. S. Santos, J. S. Lee, P. Migdal, I. C. Lekshmi, B. Satpati, and J. S. Moodera, Phys. Rev. Lett. **98**, 016601 (2007).

[10] M. Grünewald, M. Wahler, F. Schumann, M. Michelfeit, C. Gould, R. Schmidt, F. Würthner, G. Schmidt, and L. W. Molenkamp, Phys. Rev. B **84**, 125208 (2011).

[11] F. G. Monzon, H. X. Tang, and M. L. Roukes, Phys. Rev. Lett. **84**, 5022 (2000).

[12] M. Johnson and R. H. Silsbee, Phys. Rev. Lett. **55**, 1790 (1985).

[13] X. Lou, C. Adelmann, S. A. Crooker, E. S. Garlid, J. Zhang, K. S. M. Reddy, S. D. Flexner, C. J. Palmstrøm, and P. A. Crowell, Nat. Phys. **3**, 197 (2007).

[14] N. Tombros, C. Jozsa, M. Popinciuc, H. T. Jonkman, and B. J. van Wees, Nature **448**, 571 (2007).

[15] A. Riminucci, M. Prezioso, C. Pernechele, P. Graziosi, I. Bergenti, R. Cecchini, M. Calbucci, M. Solzi, and V. A. Dediu, Appl. Phys. Lett. **102**, 092407 (2013).

[16] M. Grünewald, R. Göckeritz, N. Homonnay, F. Würthner, L. W. Molenkamp, and G. Schmidt, Phys. Rev. B **88**, 085319 (2013).

[17] Z. G. Yu, Phys. Rev. Lett. **111**, 016601 (2013).

[18] P. A. Bobbert, W. Wagemans, F. W. A. van Oost, B. Koopmans, and M. Wohlgenannt, Phys. Rev. Lett. **102,** 156604 (2009).

[19] Z. G. Yu, F. Ding, and H. Wang, Phys. Rev. B **87**, 205446 (2013).

[20] Z. G. Yu, Phys. Rev. Lett. **106**, 106602 (2011).

[21] S. Maekawa, S. O. Valenzuela, E. Saitoh, and T. Kimura, *Spin Current*, (Oxford University Press, 2012).

[22] I. Žutić, J. Fabian, and S. Das Sarma, Rev. Mod. Phys. **76**, 323 (2004).

[23] Y. Kajiwara, K. Harii, S. Takahashi, J. Ohe, K. Uchida, M. Mizuguchi, H. Umezawa, H. Kawai, K. Ando, K. Takanashi, S. Maekawa, and E. Saitoh, Nature **464**, 262 (2010).

[24] E. Shikoh, K. Ando, K. Kubo, E. Saitoh, T. Shinjo, and M. Shiraishi, Phys. Rev. Lett. **110**, 127201 (2013).

[25] S. Watanabe, K. Ando, K. Kang, S. Mooser, Y. Vaynzof, H. Kurebayashi, E. Saitoh, and H. Sirringhaus, Nat. Phys. **10**, 308 (2014).

[26] V. G. Harris, A. Geiler, Y. J. Chen, S. D. Yoon, M. Z. Wu, A. Yang, Z. H. Chen, P. He, P. V. Parimi, X. Zuo, C. E. Patton, M. Abe, O. Acher, and C. Vittoria, J. Magn. Magn. Mater. **321**, 2035 (2009).

[27] Y. Y. Sun, Y. Y. Song, H. C. Chang, M. Kabatek, M. Jantz, W. Schneider, M. Z. Wu, H. Schultheiss, and A. Hoffmann, Appl. Phys. Lett. **101**, 152405 (2012).

[28] See Supplemental Material [url], which includes Refs. [29-42].

[29] T. Sakanoue, M. Yahiro, C. Adachi, K. Takimiya, and A. Toshimitsu, J. Appl. Phys. **103**, 094509 (2008).

[30] R. G. Kepler, P. M. Beeson, S. J. Jacobs, R. A. Anderson, M. B. Sinclair, V. S. Valencia and P. A. Cahill, Appl. Phys. Lett. **66**, 3618 (1995).

[31] J. Rybicki, R. Lin, F. Wang, M. Wohlgenannt, C. He, T. Sanders, and Y. Suzuki, Phys. Rev. Lett. **109**, 076603 (2012).

[32] A. Droghetti, S. Steil, N. Großmann, N. Haag, H. Zhang, M. Willis, W. P. Gillin, A. J. Drew, M. Aeschlimann, S. Sanvito, and M. Cinchetti, Phys. Rev. B **89**, 094412 (2014).

[33] W. Xu, J. Brauer, G. Szulczewski, M. Sky Driver, and a. N. Caruso, Appl. Phys. Lett. **94**, 233302 (2009).

[34] F. Burke, M. Abid, P. Stamenov, and J. M. D. Coey, J. Magn. Magn. Mater. **322**, 1255 (2010).

[35] J. Laubender, L. Chkoda, M. Sokolowski, and E. Umbach, Synth. Met. **111**, 373 (2000).

[36] M. Rosay, L. Tometich, S. Pawsey, R. Bader, R. Schauwecker, M. Blank, P. M. Borchard, S. R. Cauffman, K. L. Felch, R. T. Weber, R. J. Temkin, R. G. Griffin,

and W. E. Maas, Phys. Chem. Chem. Phys. **12**, 5850 (2010).

[37] H. Tresp, M. U. Hammer, J. Winter, K.-D. Weltmann, and S. Reuter, J. Phys. D. Appl. Phys. **46**, 435401 (2013).

[38] J. A. Weil and J. R. Bolton, *Electron Paramagnetic Resonance: Elementary Theory and Practical Applications*. John Wiley & Sons, 2007.

[39] K. Vanheusden, W. L. Warren, C. H. Seager, D. R. Tallant, J. a Voigt, and B. E. Gnade, J. Appl. Phys. **79**, 7983 (1996).

[40] F. Reisdorffer, B. Garnier, N. Horny, C. Renaud, M. Chirtoc, and T.-P. Nguyen, EPJ Web Conf. **79**, 02001 (2014).

[41] K. Harii, T. An, Y. Kajiwara, K. Ando, H. Nakayama, T. Yoshino, and E. Saitoh, J. Appl. Phys. **109**, 116105 (2011).

[42] V. Castel, N. Vlietstra, B. J. van Wees, and J. B. Youssef, Phys. Rev. B **86**, 134419 (2012).

[43] S. Wang, Y. J. Shi, L. Lin, B. B. Chen, F. J. Yue, J. Du, H. F. Ding, F. M. Zhang, and D. Wu, Synth. Met. **161**, 1738 (2011).

[44] Y. Tserkovnyak, A. Brataas, and G. E. W. Bauer, Phys. Rev. Lett. **88**, 117601 (2002).

[45] K. Ando, S. Takahashi, J. Ieda, Y. Kajiwara, H. Nakayama, T. Yoshino, K. Harii, Y. Fujikawa, M. Matsuo, S. Maekawa, and E. Saitoh, J. Appl. Phys. **109**, 103913 (2011).

[46] Y. S. Gui, N. Mecking, X. Zhou, G. Williams, and C. M. Hu, Phys. Rev. Lett. **98**, 107602 (2007).

[47] Y. Shiomi, K. Nomura, Y. Kajiwara, K. Eto, M. Novak, K. Segawa, Y. Ando, and E. Saitoh, Phys. Rev. Lett. **113**, 196601 (2014).

[48] M. Agrawal, A. A. Serga, V. Lauer, E. T. Papaioannou, B. Hillebrands, and V. I. Vasyuchka, Appl. Phys. Lett. **105**, 092404 (2014).

[49] Z. Feng, J. Hu, L. Sun, B. You, D. Wu, J. Du, W. Zhang, A. Hu, Y. Yang, D. M. Tang, B. S. Zhang, and H. F. Ding, Phys. Rev. B **85**, 214423 (2012).

[50] T. An, V. I. Vasyuchka, K. Uchida, A. V Chumak, K. Yamaguchi, K. Harii, J. Ohe, M. B. Jungfleisch, Y. Kajiwara, H. Adachi, B. Hillebrands, S. Maekawa, and E. Saitoh, Nat. Mater. **12**, 549 (2013).

[51] C. Kittel, Phys. Rev. **73**, 155 (1948).

[52] H. Kurebayashi, O. Dzyapko, V. E. Demidov, D. Fang, J. Ferguson, and S. O.

Demokritov, Nat. Mater. **10**, 660 (2011).

[53] C. W. Sandweg, Y. Kajiwara, A. V. Chumak, A. A. Serga, V. I. Vasyuchka, M. B. Jungfleisch, E. Saitoh, and B. Hillebrands, Phys. Rev. Lett. **106**, 216601 (2011).

[54] B. Koopmans, Nat. Phys. **10**, 249 (2014).

[55] Z. G. Yu, Phys. Rev. B **85**, 115201 (2012).

[56] B. Kanchibotla, S. Pramanik, and S. Bandyopadhyay, and M. Cahay, Phys. Rev. B **78**, 193306 (2008).

[57] F. J. Wang, C. G. Yang, Z. V. Vardeny, and X. G. Li, Phys. Rev. B **75**, 245324 (2007).

Figure Captions:

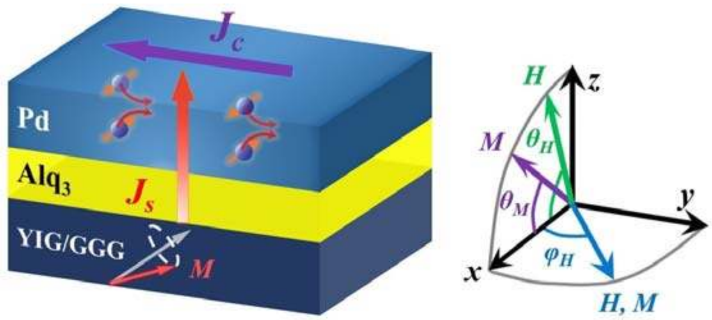

Fig. 1. Schematic of the spin pumping induced spin injection, transport and detection in a YIG/Alq_3/Pd device.

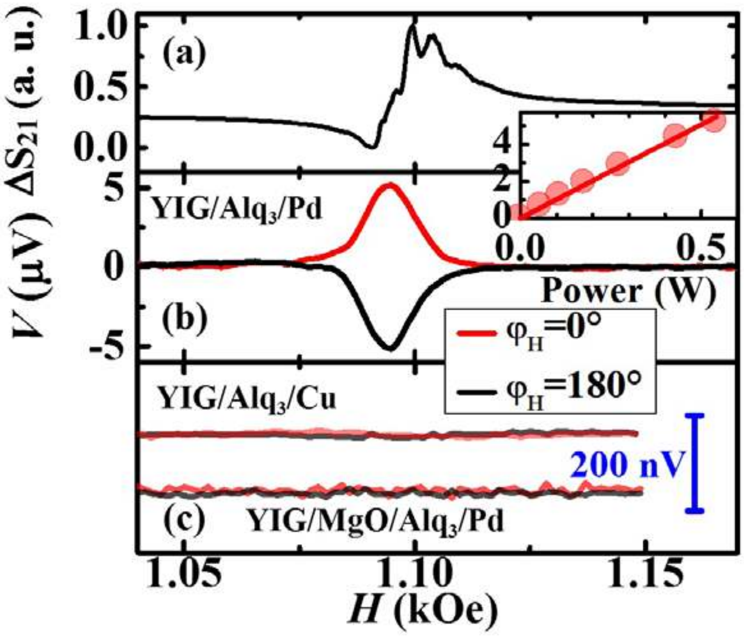

Fig. 2. (a) ΔS_{21} as a function of $\boldsymbol{H}$ for YIG/Alq$_3$ (50 nm)/Pd ($f = 5$ GHz , P_{in}=1 mW and θ_H=0°). The electric voltage as a function of $\boldsymbol{H}$ for (b) YIG/Alq$_3$ (50 nm)/Pd and (c) YIG/Alq$_3$ (50 nm)/Cu and YIG/MgO (20 nm)/Alq$_3$ (50 nm)/Pd (f=5 GHz , P_{in}=540 mW and θ_H=0°). The curves in (c) are vertically offset for clarity. Inset of (b): Microwave power dependence of V_{ISHE}, where the solid line is a linear fitting.

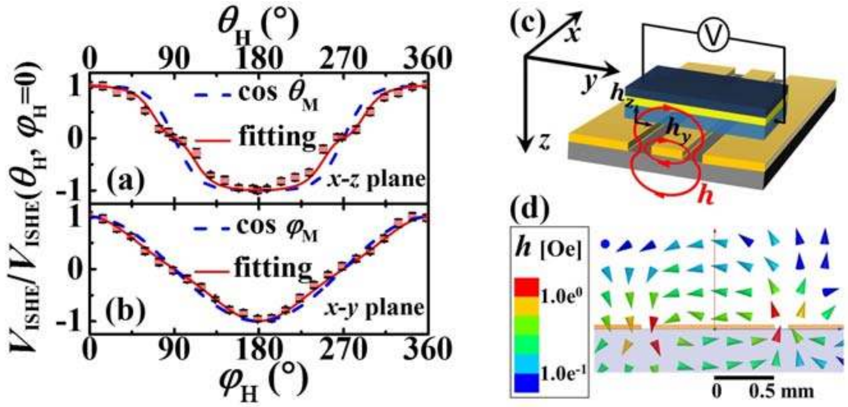

Fig. 3. Normalized V_{ISHE} as a function of (a) θ_H and (b) φ_H in YIG/Alq$_3$ (50 nm)/Pd (f =5 GHz , P_{in}=540 mW and T=300 K). The blue dash lines are the calculated results for $\cos\theta_M$ and $\cos\varphi_M$. The solid red lines are the fits utilizing Eq. (1) and (2), respectively. (c) Schematic of the experimental geometry for measurements with large samples. (d) Simulation of ***h*** distribution in the CPW.

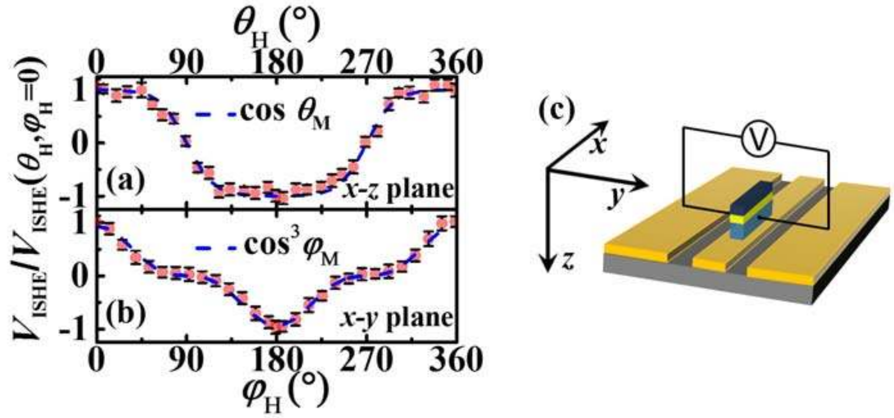

Fig. 4. Normalized $V_{\rm ISHE}$ as a function of (a) $\theta_{\rm H}$ and (b) $\varphi_{\rm H}$ for sample size smaller than the signal line of the CPW (T=300 K). The dash blue lines are the calculated curve of $\cos\theta_M$ and $\cos^3\varphi_M$. (c) Schematic of the experimental geometry for measurements with small samples.

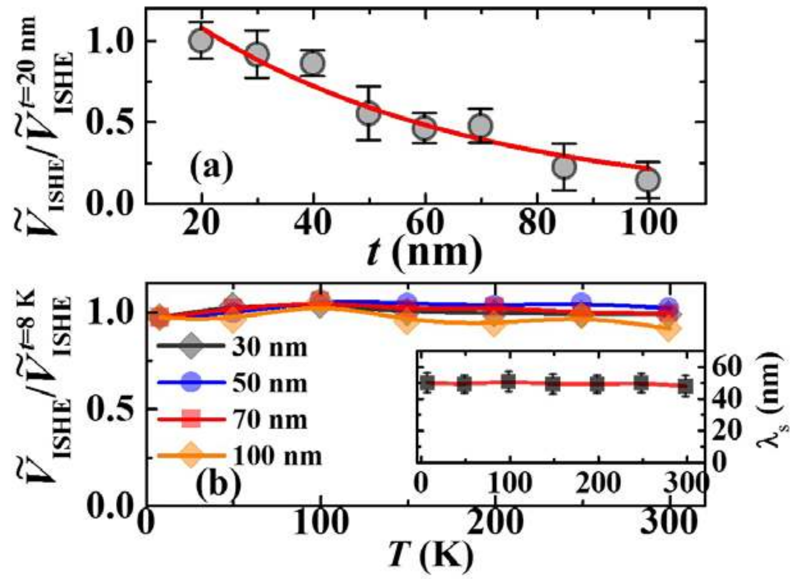

Fig. 5. (a) Normalized $\tilde{V}_{\mathrm{ISHE}}$ as a function of the Alq_3 thickness (T=300 K). The error bars are statistical errors due to the averaging of many samples. (b) T dependences of normalized $\tilde{V}_{\mathrm{ISHE}}$ for YIG/Alq_3 (t)/Pd with t=30, 50, 70 and 100 nm (f=5 GHz, P_{in}=540 mW and θ_H=0°). Inset of (b): λ_s as a function of T.